DOI: 10.13009/EUCASS2025-185
11TH EUROPEAN CONFERENCE FOR AERONAUTICS AND SPACE SCIENCES (EUCASS)

A Statistical Approach to the Design Analysis of Multimode Propulsion Systems

Davide Vetralla ⋆‡†*, Jakub Glowacki* ‡*, Stefania Carlotti* ⋆ *and Filippo Maggi* ⋆
⋆ *Department of Aerospace Science and Technology, Politecnico di Milano*
Piazza Leonardo da Vinci 32, 20133 Milan, Italy
‡ *Robinson Research Institute, Victoria University of Wellington*
68 Gracefield Rd., 5010 Lower Hutt, New Zealand
davide.vetralla@mail.polimi.it · jakub.glowacki@vuw.ac.nz

†Corresponding author

Abstract

Multimode propulsion systems, which integrate electric and chemical thrusters using a shared propellant, offer a unique capability to enhance the flexibility of in-space maneuvers while minimizing total propulsion system mass. In this work, a system-level design analysis of multimode thrusters based on a combination of monopropellant and electrothermal arcjet propulsion is presented. The results illustrate how key design optimization parameters, such as propulsion mass and transportation rate, evolve with different electric propulsion (EP) usage levels, using both deterministic analysis and stochastic methods via Monte Carlo simulations. Presented results shows that for a 500 kg payload, the total system propulsion mass varies between 500 kg and 1500 kg. The findings suggest that the use of multimode propulsion becomes advantageous only when at least 39% of the total maneuver is performed using electric propulsion. When statistical variability is considered, this threshold increases to approximately 43%. Furthermore, above an EP fraction of 49%, the predictions begin to be affected by increasing uncertainty.

1. Introduction

The combined operation of electric and chemical propulsion enables sequential delivery of both high thrust and high specific impulse for in-space missions. Such systems are designed to leverage the strengths of both propulsion types, enabling spacecraft to perform a broader range of maneuvers than would be possible with a single system alone. A defining characteristic of multimode propulsion is the use of a shared propellant between the different propulsion modes, distinguishing it from hybrid propulsion, where two or more independent systems operate separately without propellant sharing.[1] The ability to use a common propellant reservoir offers two advantages over hybrid and single systems: 1)enhanced mission flexibility; 2) propulsion system mass reduction.[2] Realization of these advantages usually comes through the optimization of spacecraft trajectories by strategically combining high-thrust and high-specific impulse propulsion at different mission phases. A variety of studies have been conducted in this direction, proposing mission profiles ranging from interplanetary transfers[3] to satellite servicing[4] relying on optimization algorithms[5] aimed at identifying the most favorable mission profiles for a given thruster architecture. At the level of thruster design, the main challenge comes with fuel compatibility, which focused research on the use of synthesized fuel using electrospray technology[6].[7] While such combinations provide a distingue advantage for micro thrusters, they are hardly scalable to larger systems and share problems typical for electrosprays such as electron backstreaming, electrochemical degradation of the propellant and overspray (which leads to the extractor or accelerator grid saturation), together with problems related to the clogging of emitters. The restrictions imposed by electrosprays have largely limited applications to niche nano and micro platforms which largely leaves multimode thrusters outside of the paragrim of small satellites. Such application, although important from the perspective of a current market share, still requires a design analysis as the extent to which multimode thrusters can be used in such platforms is not clear.

As the main benefit of multimode thrusters lies in design simplification, it becomes essential to quantify this effect through system-level analyzis. Such studies have been performed for micropropulsion systems,[2] green ionic liquids for this technology,[8] and interplanetary missions.[3] The high power application, for 500 kg payload and a ΔV=1500 m/s, showed that multimodal systems outperforms in terms of transportation rate all-chemical systems when more than 25% of the total ΔV was provided by the electric system. Furthermore, monopropellant systems were found

Copyright © 2025 by Davide Vetralla, Jakub Glowacki, Stefania Carlotti, and Filippo Maggi. Published by the EUCASS association with permission.

to be more efficient than bipropellant systems, offering reduced system mass and shorter burn durations, despite having 33% lower specific impulse and only one-tenth the thrust. The monopropellant/pulsed inductive thrusters system achieved the lowest total system mass, while the monopropellant/arcjet system demonstrated the highest transportation rates across all possible chemical/electric ΔV ratios. This study was later expanded to include lower payload masses for a variety of novel green propellants,[9] like ADN-based LMP-103S, HAN-based SHP-163 and FAM-110A. Results showed that for a baseline 250 kg spacecraft, Hall effect thrusters provide the best balance, offering 9.4% to 35.5% more ΔV than arcjets and ion thrusters; furthermore, LMP-103S outperforms other propellants, with ΔV gains of up to 13.5%. While this comprehensive analysis provides an overview of the theoretical benefits of using multimode propulsion with alternative propellants, the realization of hydrazine driven Hall-effect thruster is a novel and complex concept and due to due to channel erosion or low efficiency and instabilities[10] will require significantly more time to be considered a viable candidate. As such, current understanding lacks focus on the level of technologies that would have a technological readiness level that would allow physical realization. Such analysis would need to target a combination of electrothermal-monopropellant thrusters for a variety of propellants, and mission scenarios. The electrothermal thrusters are much simpler and offer greater flexibility in terms of propellant use.[11] Another aspect, that is still not understood is the role of uncertainties in the thruster design. The combination of two technologies that have a different dependency on design parameters could lead to a nonuniform impact of parameter uncertainties on the total mass of the system - a feature that will only manifest itself in multimode configuration. These two aspects require further analysis before conclusions can be drawn on the potential applicability of multimode thrusters.

2. Methodology

Spacecraft maneuvers are governed by the Tsiolkovsky rocket equation. However, the original form of this equation needs to be modified[10] to take into account, different types of thrusters—such as chemical and electric both characterized by their specific impulse ($I_{sp,chem}$ and $I_{sp,elec}$). Because I_{sp} directly affects the mass conversion to velocity, the total maneuver must be broken down into segments corresponding to each propulsion mode. Thus, the rocket equation must be applied separately to each segment of the maneuver—one equation for the portion performed by the chemical thruster and another for the portion executed by the electric thruster. The total propellant required is then determined by combining the results of these successive applications of the rocket equation.

By defining a parameter representing the electric propulsion usage fraction as the total ΔV executed by electric propulsion

$$EP = \frac{\Delta V_{elec}}{\Delta V}, \tag{1}$$

it is possible to express the Tsiolkovsky rocket equation for multimode systems as

$$\frac{m_f}{m_0} = e^{\frac{-\Delta V}{I_{sp,mm} g_0}} = e^{\frac{-\Delta V}{g_0}\left[\frac{1-EP}{I_{sp,chem}} + \frac{EP}{I_{sp,elec}\eta_v}\right]}, \tag{2}$$

where m_0 denotes the initial total mass and m_f the final mass after the complete maneuver,$I_{sp,mm}$ the effective specific impulse and η_v mission planning efficiency (for details refer to[12]). In this study $\eta_v = 1$, the parametric studies on the role of mission planning efficiency can be found in.[13]

Analogically, it's possible to derive an expression for the ratio of chemical ($m_{prop,chem}$) to electric ($m_{prop,elec}$) propellant as a function of the specific impulses of each mode and the EP usage fraction

$$\frac{m_{prop,elec}}{m_{prop,chem}} = \frac{1 - e^{\frac{-\Delta V}{I_{sp,mm} g_0}}}{1 - e^{\frac{-(1-EP)\Delta V}{I_{sp,chem} g_0}}} - 1. \tag{3}$$

Then, the mass of propellant required to accelerate a spacecraft through a desired velocity change can be calculated from a rearranged form of the rocket equation

$$m_{\mathrm{prop}} = \frac{m_{\mathrm{pay}}\left(e^{\frac{\Delta V}{I_{\mathrm{sp,mm}}\, g_0}} - 1\right)\left(1 - \frac{m_{inert}}{m_{inert} + m_{prop}}\right)}{1 - \frac{m_{inert}}{m_{inert} + m_{prop}}\, e^{\frac{\Delta V}{I_{\mathrm{sp,mm}}\, g_0}}}, \tag{4}$$

where m_{pay} and m_{inert} are payload and inert masses respectively. The inert mass is composed of the propellant and pressurizer tanks (m_{tank}) (if needed), propellant feed lines and valves (m_{lines}) , thruster (m_{thruster}), power processing unit

(m_{PPU}), solar panels (m_{SP}) and structural mounts for the propulsion system (m_{struct}) . Out of all the inert masses,m_{tank}, m_{struct}, m_{lines}, were common to the whole system. The tanks' mass were calculated using semi-empirical formula[14]

$$m_{tank} = \frac{P_{burst}\, m_{prop}}{g_0\, \Phi_{tank}\, \rho_{prop}}, \tag{5}$$

where the burst pressure P_{burst} is assumed to be 1.25 times the tank pressure and Φ_{tank} is an empirical tank sizing parameter chosen to be 2500 m for the hydrazine tanks, as it corresponds to stainless steel.[10] The propellant density ρ_{prop} is chosen to be 561 kg/m^3, which corresponds to the density of ammonia (which is the main product of hydrazine decomposition in a gaseous state, which may occur during long time storage[15]) at a storage pressure of 300 psi.[10]
The mass of lines and valves is estimated as 50% of the thruster mass $m_{\text{lines}} = 0.5 m_{\text{thruster}}$, (for each one of the two) a value typical of spacecraft thrusters historically.[1] The mass of structural mounts is assumed to be 10% of the total inert mass $m_{\text{struct}} = 0.1 m_{\text{inert}}$.[10] In the numerical formulation, after including all masses specific to propulsion units, the solution to Eq. 4 was found iteratively. The reason for the use of hydrazine as a propellant of choice, throughout this study, was to create a study case scenario that could be comparable with the literature.

2.1 Monopropellant

To model the monopropellant and estimate the chemical specific impulse, the NASA CEA code[16] was employed. Specifically, it was used to compute the specific heat capacity at constant pressure (c_p), the specific heat ratio (γ), and the final combustion temperature T_{cc}. The program was executed by selecting liquid hydrazine as fuel (N_2H_4 (L)) and assuming an initial temperature of 300 K. Thruster performance was esimtaed using, equations:

$$C_F = \lambda \sqrt{\frac{2\gamma}{\gamma-1}\left(\frac{2}{\gamma+1}\right)^{\frac{\gamma+1}{\gamma-1}}\left[1-\left(\frac{P_e}{P_c}\right)^{\frac{\gamma-1}{\gamma}}\right]} + \frac{P_e}{P_c}\varepsilon, \tag{6}$$

$$\frac{1}{\varepsilon} = \left(\frac{\gamma+1}{2}\right)^{\frac{\gamma-1}{\gamma}}\left(\frac{P_e}{P_c}\right)^{\frac{1}{\gamma}}\sqrt{\frac{\gamma+1}{\gamma-1}\left(1-\left(\frac{P_e}{P_c}\right)^{\frac{\gamma-1}{\gamma}}\right)}, \tag{7}$$

given a known expansion ratio ($\epsilon = 200$) and combustion chamber pressure P_c (300 Psi[10]). In Eq. 6, the divergence correction factor has been added

$$\lambda = \frac{1}{2}\left(1 + \cos(\alpha)\right), \tag{8}$$

where half cone divergence angle α was assigned as 15 deg.
The pressure ratio was determined iteratively using Eq. 7, where the equation is set equal to zero to search for the roots. This process starts with an initial guess and refines it iteratively based on the value of the equation. The function continues to adjust the guess until the results converge, meaning the solution is sufficiently close to zero, within a specified tolerance (10^{-6}).
The characteristic velocity (c^*) was computed following equation,[17]

$$\begin{cases} c^* = \dfrac{\sqrt{R^*\, T_{\text{cc}}\, \gamma}}{\Gamma}, \\[2ex] \Gamma = \gamma\left(\dfrac{2}{\gamma+1}\right)^{\dfrac{\gamma+1}{2(\gamma-1)}}, \\[2ex] R^* = c_p\left(1-\dfrac{1}{\gamma}\right). \end{cases} \tag{9}$$

where R^* is the specific gas constant. Finally, the specific impulse was found using

$$I_{sp,chem} = \frac{c^*\, c_F}{g_0}. \tag{10}$$

This approach yielded a chemical specific impulse of $I_{sp,\text{chem}} = 234.59$ s (which can be verified against reference value of 243.0 s,[10] leading to a relative difference of 3.46%). To validate this result, it was compared against six real-world monopropellant examples sourced from the literature.[10, 17–20] These references include various types of monopropellants, primarily hydrazine (N_2H_4) and hydrogen peroxide-based formulations with concentrations ranging

DOI: 10.13009/EUCASS2025-185

from 80% to 89%. In all cases, the computed values were found to be within 5% of the reported data (the results are reported in Table 1), indicating a high level of consistency and reliability. This level of accuracy is considered satisfactory for a feasibility study and confirms the validity of the chosen modeling approach. Although the specific impulse of hydrazine monopropellants is well known, this step allowed validation of the tool, which could be used for a range of different propellants, as well as for estimating model uncertainty.

Configuration	**Reference I_{sp} [s]**	**MMP I_{sp} [s]**	**Error [%]**
H_2O_2 80%	160.00	152.06	4.96
H_2O_2 89 %	175.30	176.95	0.94
Monarc 1 (Hydrazine)	235.00	228.77	2.65
Monarc 5 (Hydrazine)	230.00	235.15	2.24
Monarc 22-6 (Hydrazine)	228.00	231.62	1.59
Monarc 445 (Hydrazine)	235.00	227.31	3.27

Table 1: Comparison between MMP results and reference data for various monopropellants

The total tank pressure was calculated as the sum of the combustion chamber pressure and the various pressure losses occurring along the feed system.

$$\Delta P_{\text{dyn}} = \frac{1}{2}\rho v^2, \quad [Pa] \tag{11}$$

$$\Delta P_{\text{cool}} = 0.15\, P_{\text{cc}}, \quad [Pa] \tag{12}$$

$$\Delta P_{\text{inj}} = 0.2\, P_{\text{cc}}, \quad [Pa] \tag{13}$$

$$\Delta P_{\text{feed}} = 40000, \quad [Pa] \tag{14}$$

$$P_{\text{tank}} = P_{\text{cc}} + \Delta P_{\text{dyn}} + \Delta P_{\text{cool}} + \Delta P_{\text{inj}} + \Delta P_{\text{feed}}. \quad [Pa] \tag{15}$$

where, according to the literature:[21]

- ΔP_{dyn} is the dynamic pressure loss due to propellant motion through the feed lines. It assumes a flow velocity of approximately 10 m/s;
- ΔP_{cool} accounts for pressure losses in the cooling jacket, typically ranging from 5% to 25% of the combustion chamber pressure, depending on the regenerative cooling design;
- ΔP_{inj} represents pressure losses across the injector, generally estimated between 5% and 30% of P_{cc}, with 20% being a common assumption for unthrottled systems;
- ΔP_{feed} includes pressure losses in the feeding lines and valves, typically between 35 and 50 kPa, depending on system complexity and routing.

Estimated tank pressure found was 28 atm, compared to the 25 atm used in literature.[10]
The mass of the thruster was, estimated based on the mass of the decomposition chamber (subscript "c") and the nozzle (subscript "e" used for exit dimensions) $m_{\text{thruster}} = m_c + m_{\text{nozzle}}$. The nozzle throat (subscript "t") area was calculated from

$$A_t = \frac{T}{C_F P_{cc}}, \tag{16}$$

using a fixed thrust[10] (T) and a thrust coefficient from Eq. 6. The thrust chamber geometry was calculated through empirical formulas:[14]

$$A_c = A_t\,(\,8\,D_t^{-0.6} + 1.25), \tag{17}$$

$$L_c = L^*\,\frac{A_t}{A_e}, \tag{18}$$

where a characteristic length, L^*, of 2.5 is chosen for monopropellant thrusters.[10] The wall thickness t_w and the mass of the combustion chamber m_c is estimated using:

$$t_w = \frac{P_{burst}\,D_t}{2F_{tu}}, \tag{19}$$

$$m_c = \pi\,\rho_t\,t_w\left[2r_t\,L_c + \frac{r_t^2 - r_e^2}{\tan\theta_{cc}}\right]. \tag{20}$$

DOI: 10.13009/EUCASS2025-185

For this system-level analysis, the burst pressure is twice the chamber pressure, and the decomposition chamber is made of columbium (F_{tu} = 310 MPa, ρ_t = 8600 kg/m^3).[10] The angle of the convergence section θ_c is set to 45 deg, recognizing that it typically comprises only a small percentage of the total thruster mass[10] The mass of the nozzle m_{nozzle} was estimated using[17]

$$\begin{cases} L_{\text{nozzle}} = \dfrac{D_e - D_t}{2\tan(\theta_{cc})}, \\ m_{\text{nozzle}} = \pi \rho_{cc}\, t_w\, L_{\text{nozzle}} \left(\dfrac{D_e}{2} + \dfrac{D_t}{2}\right). \end{cases} \tag{21}$$

2.2 Arcjet

To accurately estimate the inert masses in an arcjet thruster, the methodology outlined in[17] was employed. This approach incorporates various aspects of the thruster by using efficiency factors (η) and specific mass coefficients (β)—expressed in kg/W—sourced from literature.[9,17,22,23] The advantage of working with specific mass is that usually, the system design involves many components, all of which process powers proportional (through efficiency factors) to the power P. It's then possible to compute the total specific mass by summing the component values (with the weighting factors due to efficiencies)

$$m_{\text{inert},elec} = \beta_{th} \cdot \frac{P_j}{\eta_{th}} + \beta_{pp} \cdot P_{pp} + \beta_s\, P + \beta_H \cdot P_H, \tag{22}$$

with:

$$\begin{cases} \eta_{\text{tot}} = \eta_{\text{th}}\, \eta_{\text{pp}}\, \eta_{\text{s}}, \\ P_j = \eta_{\text{tot}}\, P, \\ P_{\text{pp}} = \eta_s\, P, \\ P_H = (1-\eta_s)\, P + (1-\eta_{\text{pp}})\, P_{\text{pp}} + K\, \dfrac{(1-\eta_{\text{th}})\, P_j}{\eta_{\text{th}}}, \end{cases} \tag{23}$$

where, the subscript "pp" refers to the power processing system, "H" to the heat rejection system, "s" to the power source, and "th" to the thrust system. The factor K accounts for the fact that only a fraction of the power loss in the thruster needs to be handled by the heat rejection system; the rest is either expelled with the exhaust or radiates locally. In some cases, this factor may reasonably approach zero.[17]

In Eq. 22 and Eq. 23, η_{th} represents the thrust efficiency (usually around 0.4 for an arcjet), indicating the conversion of electrical power into thrust power. η_{s}, on the other hand, represents the efficiency of converting power from the source to electricity: for photovoltaic array systems, the output is already in the form of electricity, so $\eta_{\text{s}} = 1$. The power processor efficiency, η_{pp}, is typically very high, ranging from 97% to 99%.

Finally, by knowing β_s (assumed equal to 0.008 kg/W[24]) and the power over area ratio (200 W/m^2 - value assumed as a good trade-off value between silicon-based cells of 180 W/m^2 and gallium arsenide 220 W/m^2[17]) of solar panels it's possible to compute their mass and area: for P = 30 kW, they are 240 kg and 150 m^2 respectively. These results are in agreement with the current technological readiness level of solar panels inferred from the open literature.[25–27] To provide a sense of scale, it is worth noting that systems of this size are uncommon and can be compared only to the largest electric propulsion missions to date, such as the *Europa Clipper*, which was designed with 102 m^2 solar panels[28]).

2.2.1 Performances

The second step involved refining the approach by developing a tool to predict performance, thus eliminating the need to rely solely on literature. This was achieved through the use of NASA's CEA Code. Specifically, the tool was applied similarly to a monopropellant system, calculating parameters such as the specific heat ratio γ, specific heat capacity c_p, and the final temperature T_1, all assumed as constant. With the mass flow rate kept constant as in,[10] along with the input power P and efficiency η, the new final temperature was then computed using the following equations:

$$\begin{cases} \Delta H = \dfrac{P \cdot \eta}{\dot{m}}, \\ T_2 = T_1 + \dfrac{\Delta H}{c_p}. \end{cases} \tag{24}$$

The flow chart of the simulation and integration of the CEA Code is presented in Fig:1. Finally, by using the same

DOI: 10.13009/EUCASS2025-185

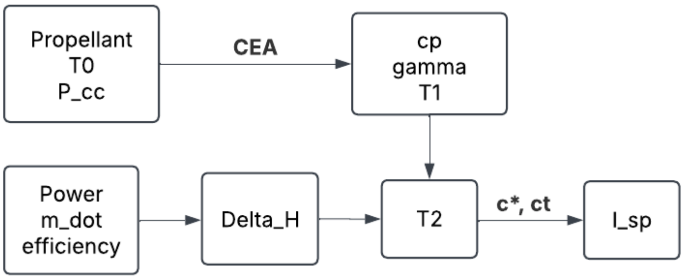

Figure 1: Block Diagram of computation of $I_{sp,elec}$

procedure as mentioned in subsection 2.1, the $I_{sp,elec}$ was computed though c^* and c_F. The results, along with the verification against the literature[10] are shown in Table 2. The direct comparison between the numerical results shows good agreement between the numerical approaches with the relative error of 1%.

Propellant	**Power [kW]**	$\dot{m}$ **[mg/s]**	η	$I_{sp,expected}$ **[s]**	$I_{sp,computed}$ **[s]**	**ERR** [%]
Hydrazine	30	281.8	0.28	787	794.71	**1.00**

Table 2: Results of Arcjet's performances via MMP Code

2.2.2 Validation

The validation campaign was carried out following two steps. First, a database of arcjet thrusters operating with various propellants and power levels was identified.[11] The input power of the analyzed thrusters ranged from 0.5 to 20 kW, while $\dot{m}_{prop}$ from 13 to 50 mg/s. All the reported results were successfully reproduced using the approach described earlier, and they are shown in Fig. 2 where it is possible to observe a good agreement between the model and measurements, with an average error of 4.267% and a standard deviation of 4.575.

Next, a separate experimental study focusing on hydrogen arcjets with power levels ranging from 5 to 30 kW, was evaluated;[29] the results are presented in Fig. 3. The relative error was just 0.821%; the noticeable drop of I_{sp} at 29.9 kW is to be attributed to the specific energy introduced into the system, going from around 340 to around 250 MJ/kg (and then back up to 340). This low error may be attributed to the simplicity of hydrogen as an element, which minimizes the likelihood of chemical reactions during operation. For this reason, it is important to note that such favorable results will not generalize to more complex propellants.

The accurate result obtained helps to justify this approach and the assumptions made — such as treating both γ and c_p as constant, assuming that all the gas passing through the arc reaches the temperature T_2, and neglecting any alterations to the flow due to plasma formation or interaction.

2.3 Cost Function: Transportation Rate

The transportation rate TR was chosen as a cost function for this study and is defined as the additional payload mass capacity gained by using an electric burn compared to an all-chemical burn, divided by the increase in burn time, as shown in

$$TR = \frac{m_{pay,mm} - m_{pay,allchem}}{t_{b,mm} - t_{b,allchem}} \quad [kg/day]. \tag{25}$$

This parameter helps to assess the trade-offs between adopting a multimode propulsion system and relying solely on chemical propulsion. While electric propulsion can reduce the required propellant mass due to its higher specific impulse, it also increases inert mass (primarily because of additional components such as solar panels) and extends the time needed to achieve the required ΔV. In the presented study it is also important to understand that an all-chemical system does not simply refer to an EP fraction of zero, but rather to a scenario where the spacecraft contains no EP components (no thrusters, no cables, no solar array). When computing this parameter, the problem needs to be reconstructed by changing the constraints: the mission shifts from a fixed deliverable payload mass ($m_{payload}$) to a fixed total initial mass (m_0), both with the same total ΔV.[10]

DOI: 10.13009/EUCASS2025-185

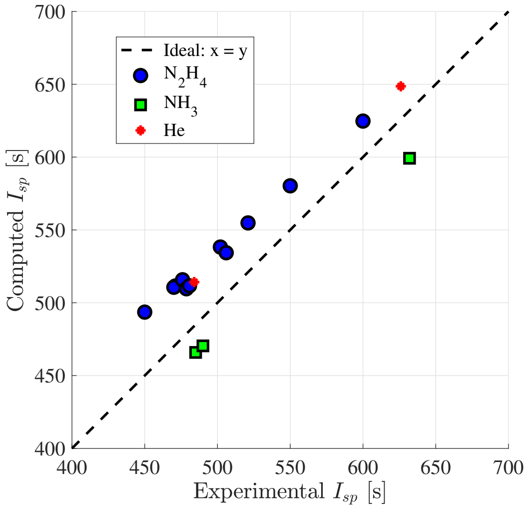

Figure 2: Correlation between Experimentally measured I_{sp}[11] and computed values

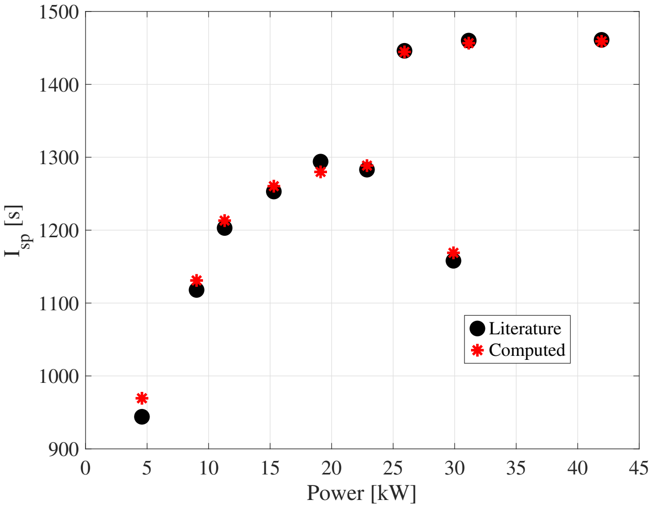

Figure 3: Correlation between Experimentally measured I_{sp}[29] and computed values

3. Results

In this section, the results obtained using the numerical formulation are presented alongside those from the literature,[10] enabling a direct comparison and highlighting the impact of the different methodologies. Therefore, all the conditions were set to mimic results presented in the literature, replicating a typical LEO - GEO orbit transfer with m_{pay} = 500kg, $P_{electic}$ = 30kW, ΔV = 1500m/s. In all presented results, the proposed numerical formulation is referred to as an MMP (Multimode propulsion) code.

In Fig. 4, the equivalent specific impulse, obtained through Eq. 2, is shown based on the initial values of $I_{sp,\text{chem}}$ and $I_{sp,\text{elec}}$ derived from the two previously described approaches. Since these initial values are very similar, the behavior of $I_{sp,\text{mm}}$ closely follows the trend predicted in the literature.

A different trend emerges when considering the total mass of the propulsion system (including propellant mass) as a function of the electric propulsion fraction (EP fraction), as shown in Fig. 5. Here, a discrepancy of approximately 200 kg at EP = 1 and nearly 400 kg at EP = 0 becomes evident. Given the near-identical specific impulse values, this mass difference is primarily attributed to disparities in the inert mass components. This hypothesis is confirmed in

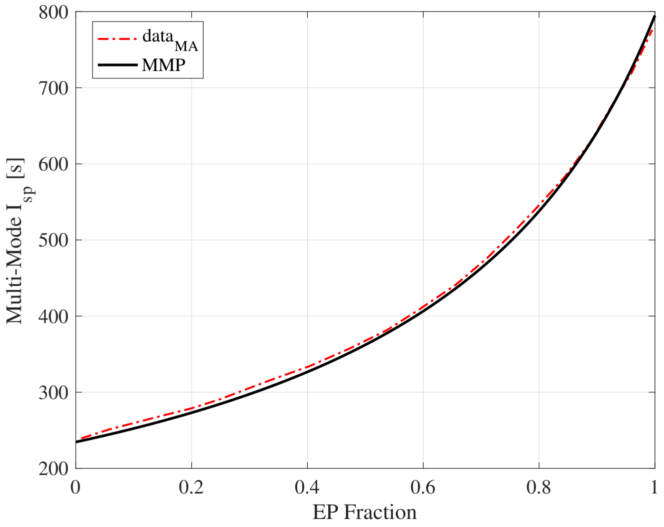

Figure 4: Multimode Specific Impulse

DOI: 10.13009/EUCASS2025-185

Fig. 6, which isolates the inert masses of the system. The discrepancy is largely due to an underestimation of the electric propulsion system's inert mass in the estimation from the literature. In contrast, the chemical propulsion system's inert mass estimates were nearly identical across both approaches. One of the major contributors to this difference is the solar array: in the literature, its mass was estimated at 90 kg using scaling laws proportional to the power required, while the alternative method, based on a specific mass coefficient, yielded a value of 240 kg. From what was found in the literature, treating high-power solar panels, the power density needed to deliver 30 kW of power with a mass of 90 kg does not exist.

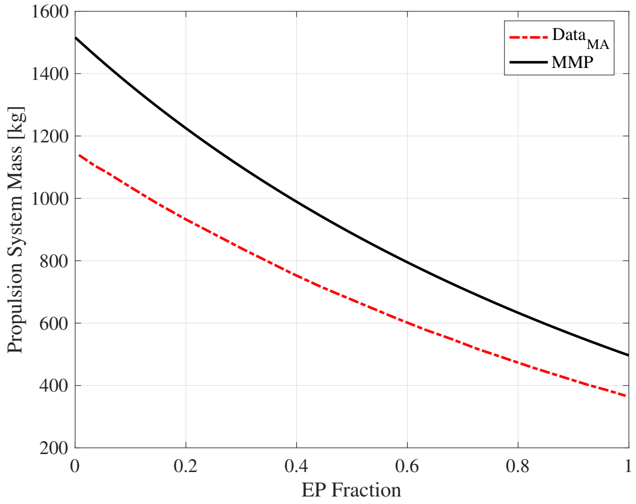

Figure 5: Cross comparison of total propellant masses between the MMP code and simulation from the literature[10]

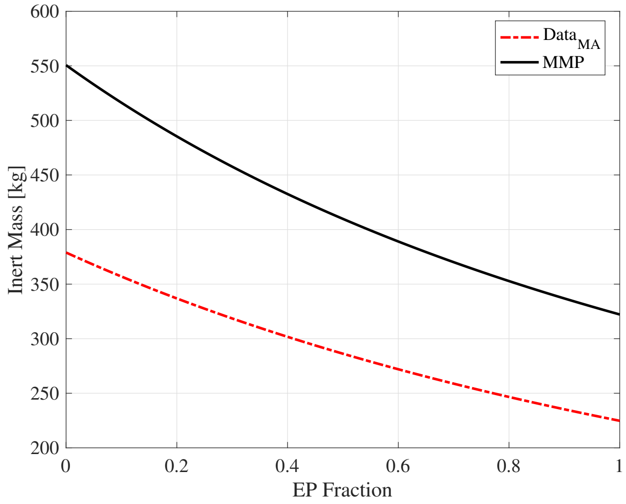

Figure 6: Cross comparison of total inert masses between the MMP code and simulation from the literature[10]

m

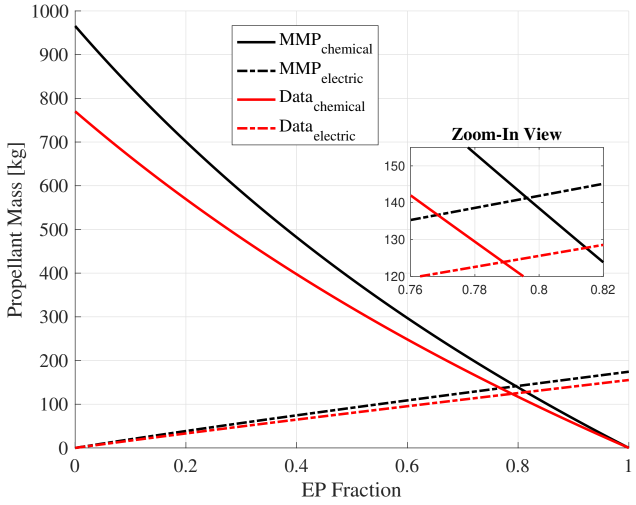

Figure 7: Cross comparison of propellant masses between MMP code and simulation from literature[30]

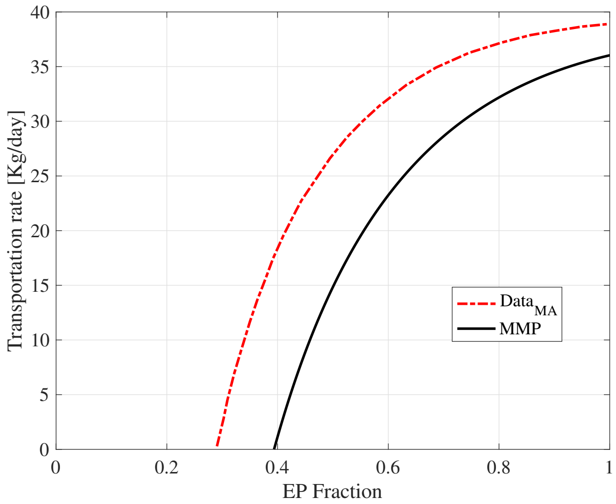

Figure 8: Cross comparison of TR between MMP code and simulation from literature[10]

Fig. 7 presents the breakdown of propellant mass requirements for both chemical and electric propulsion systems as a function of the electric propulsion fraction. As expected, increasing the EP fraction leads to a reduction in chemical propellant mass and a corresponding increase in electric propellant mass. The total propellant mass decreases with higher EP fractions due to the higher specific impulse of electric propulsion ($I_{sp,\text{elec}}$) compared to chemical propulsion ($I_{sp,\text{chem}}$). However, at $EP = 0$, a discrepancy of approximately 200 kg in total propellant mass between the two spacecraft is observed. This difference is primarily due to the significant variation in inert mass: the lower specific impulse of the chemical system amplifies the influence of structural and non-propellant mass on the total propellant requirement. The inset plot offers a zoomed-in view around $EP \approx 0.8$, highlighting the point at which the total

DOI: 10.13009/EUCASS2025-185

propellant mass is equally split between chemical and electric propulsion. Fig. 8 illustrates the variation in TR obtained using the two different codes. Due to the higher total propulsion system mass associated with the MMP method, the TR remains negative until higher EP fractions (positive only beyond approximately $EP_{critical}$ = 0.4). As EP increases, the discrepancy in TR between the two methods progressively diminishes, decreasing from roughly 17 kg/day at EP=0.4 to approximately 1.7 kg/day.

4. Uncertainty Analysis

The results presented in the previous section discuss the consequences of using the multimode system for different usage of electric thruster, but they come with limitation related to its deterministic character, and as such can only be treated as a baseline. As the role of the input variables and their uncertainties may vary for different usage of multimode thrusters it becomes crucial to understand their distribution for different operating conditions (usage of electric propulsion). For this purpose, considering inherent nonlinearities of the model a statistical method based on Monte Carlo Analysis was used.[31]

Specifically, the analysis focuses on modeling uncertainties of two key input parameters: the specific impulses for chemical and electric propulsion. Other factors, such as combustion chamber pressure and propellant density, were assumed to have a secondary effect, mainly on the masses of the subsystems. The result enabled isolation of the role of uncertainties in the prediction of thrusters performance of two cost function - total mass of the system and the transportation rate.

For $I_{sp,chem}$, a uniform distribution provides a good approximation, as stated in the literature.[32] For high-area-ratio rocket nozzles, the total uncertainty associated with I_{sp} has been reported to be 3% (expressed as coefficient of variation). Therefore, in this study, $I_{sp,chem}$ is set equal to $235.40 \pm 3.06s$. Uncertainties of $I_{sp,elec}$ were assigned using a similar approach, based on the model uncertainty. More specifically, a normally distributed random error (as described in Section 2.2.2) was added to the mean specific impulse value computed using the MMP Code ($I_{sp,elec,mean}$ = 794.71 s). As a reminder, the error found had μ_{err} = 4.267% and σ_{err} = 4.575.

It is important to note that the values used are sourced from the literature and are subjected to their own inherent parameter uncertainties. The measurements are not entirely accurate due to limitations of the measurement instruments and as such are not know deterministically. As a result, a necessary extension of this analysis is to incorporate these parametric uncertainties into the input parameters of the model implemented in the numerical model.

4.1 Numerical convergence

The precision of the Monte Carlo method depends on the population size chosen. In general, a larger population yields more accurate statistical results; however, this comes at the cost of increased computational effort.[33] To determine an appropriate population size, an analysis was conducted using the sample mean and estimated standard deviation. In order to estimate these sample error, at every iteration, the script computes a new value of total mass and transportation rate, then it updates their respective mean and standard deviation using all previous iterations; finally, it computes the change in percentage with respect to the previous iteration. From Fig. 9 - 12, it's possible to visualize the effect of the sample size (number of iterations) on the stability of the mean and standard, for both the total mass of the propulsion system (Fig. 9-10) and the transportation rate. Results presented in Fig. 11-12 show only the EP fraction that lead to a positive TR (Fig. 11-12).

Across all cases, presented in Fig. 9-10, the mean values settle typically within the first few hundred iterations. The standard deviation takes longer to stabilize, especially for the TR, but it eventually levels off. Overall, the system shows reliable convergence behavior, and the choice of EP clearly affects both how fast and how consistently that convergence happens. To guarantee a stable enough outcome,[34] the number of iterations was set to 10^3, which yielded a stable standard deviation with an error of approximately 0.5% after about thirty seconds of computation.

4.2 Correlation

Fig: 13-14 explore how the relationship between specific impulse and key mission parameters shifts depending on how much electric propulsion is used. The data was processed using the correlation function, which calculates coefficients from zero to one over a range of EP fractions, and quantifies the dependency between input and output. This approach helped to visualize which variables are most influenced for every EP fraction.

More specifically, Fig. 13 shows how $I_{sp,chem}$ and $I_{sp,elec}$ relate to four key variables: total mass, chemical and electric propellant masses, and transportation rate. At low EP fractions, an increase in $I_{sp,\mathrm{chem}}$ leads to a reduction in total mass and chemical propellants. However, as the share of electric propulsion grows, this trend diminishes. On the other hand, $I_{sp,\mathrm{elec}}$ starts to play a more significant role, especially because of its strong and consistent positive

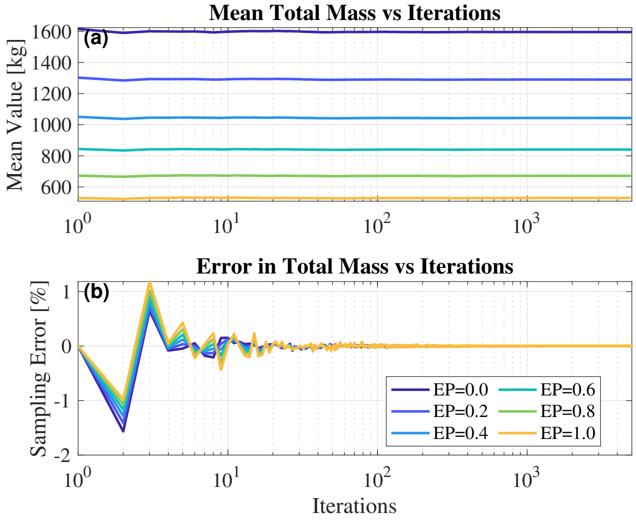

Figure 9: Convergence of μ for Total Mass

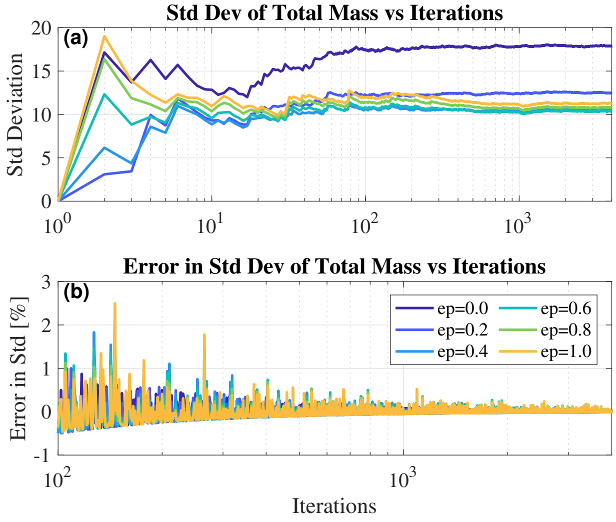

Figure 10: Convergence of σ for Total Mass

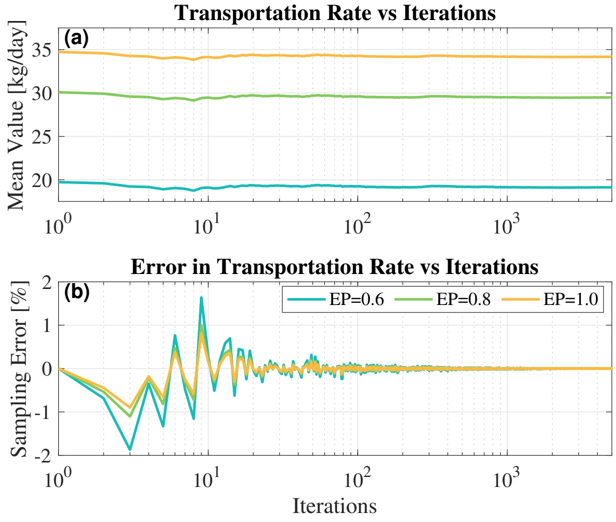

Figure 11: Convergence of μ for Transportation Rate

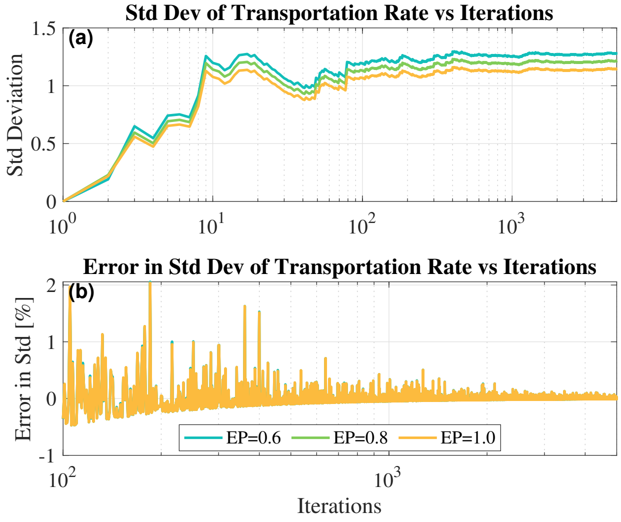

Figure 12: Convergence of σ for Transportation Rate

correlation with transportation rate. This correlation is even stronger—in absolute terms—than the one observed with $I_{sp,\text{chem}}$. This suggests that if the goal is to increase transportation rate, improving $I_{sp,\text{elec}}$ would be the more effective strategy. Additionally, the negative correlation between $I_{sp,\text{chem}}$ and transportation rate can be understood by considering how transportation rate is defined. Since it compares the performance of a multimode propulsion system to that of a purely chemical one, increasing $I_{sp,\text{chem}}$ makes the two systems more similar, thereby reducing the relative benefit and lowering the transportation rate.

Finally, as shown in Fig. 14, the relationship between the two specific impulses and both the total mass of the propulsion system and TR becomes much clearer and more intuitive. From this figure, it is evident that the strength of the correlation between the two specific impulses (I_{sp}) and the total mass (m_{tot}) changes gradually as the EP fraction increases. A noticeable shift occurs just before an EP fraction of 0.4: prior to this point, $I_{sp,chem}$ has a greater influence than $I_{sp,elec}$, whereas after this threshold, the situation reverses. This shift does not occur exactly at an EP fraction of 0.5, but rather before it.
As for the TR, the correlation does not change for the EP fraction above 0.2. Above TR of 0.3 both correlation flattens and the results shows to be strongly dependent on $I_{sp,elec}$, characteristics that doesn't change with the increase in EP fraction. Considering that only values of TR above 0.4 are of interest from the operational point of view (TR becomes positive as shown in Fig. 8), $I_{sp,elec}$ has the highest influence on TR for all practical implementations.

DOI: 10.13009/EUCASS2025-185

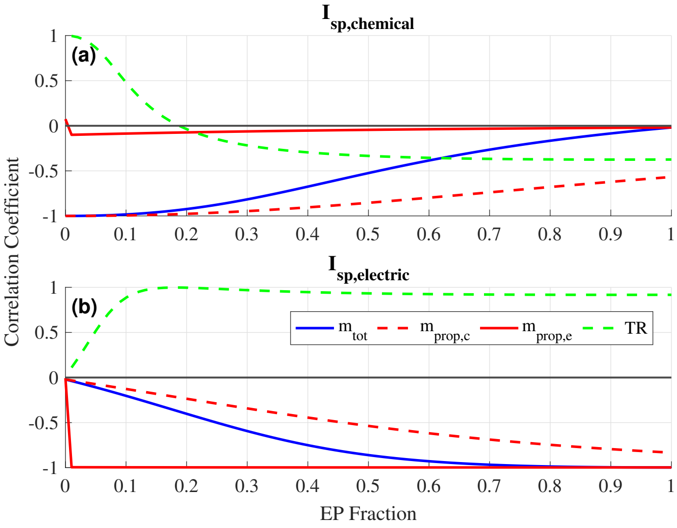

Figure 13: Correlation of specific impulse with propellant masses and transportation rate

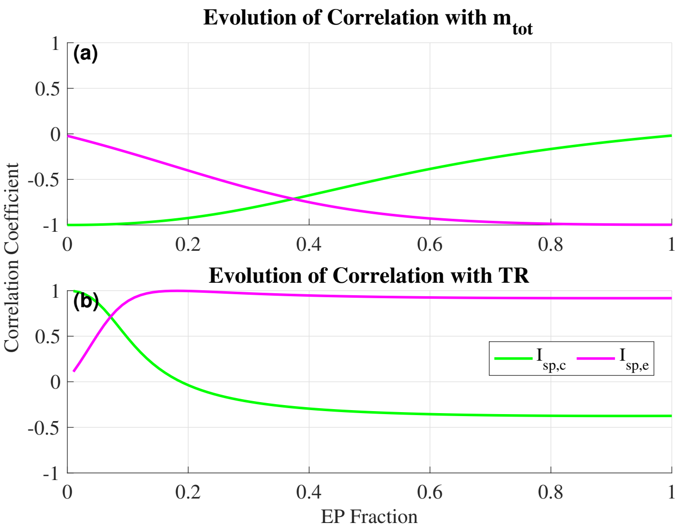

Figure 14: Correlation of Transportation Rate and Total Mass

4.3 Evolution of Uncertainties

To consolidate the analysis, the results are presented in terms of the probability distributions for different EP fractions (Fig. 15). This visualizes the evolution of distribution functions and could provide additional insight into design scenarios. The assumption was made that the design should represent a high (> 99%) confidence level and is represented as 3σ. Fig. 15a presents probability distribution of chemical, total ale electric propulsion masses in the function of EP fraction. Fig. 15b presents probability distribution of *TR* in the same domain. As shown on Fig. 15b addition of the confidence level to the design analysis increases the EP fraction for which TR becomes positive to $EP_{critcal} = 0.43$.

Additionally, to better understand the behavior of these uncertainties, the 3σ bounds for the total mass and *TR* were plotted in Fig. 16, along with their corresponding slopes. The plot shows that the uncertainties of *TR* remain nearly constant, with a derivative of zero over most of the EP fractions. More notably, the slope for the total mass shows a change in sign at an EP fraction of 0.49. This suggests that uncertainties decrease up to this point, after which they begin to increase again as the EP fraction increases. This point can be considered a potential design optimum, as it corresponds to the configuration that minimizes uncertainties. Fig. 17 shows how the propulsion system behaves when real-world uncertainties in performance are taken into account and bound previously presented evolution of 3σ region, with the shape of the probability distribution and the cumulative probability functions. Fig. 17 reveals that for all EP fractions, the probability functions can be approximated with the Gaussian distribution. The effect previously presented in Fig. 16b, where the scattering of the results was presented, is visualized using probability distributions. It can be seen that 17b follows closely the probability distribution function and could be associated with the lowest uncertainties. After that, as shown in Fig. 17c, the results become spread. The absolute values of σ can be found in Table 3.

	EP=0.2	EP=0.5	EP=0.8
μ	1287.25	942.04	672.87
σ	12.41	10.39	10.96

Table 3: Probability of Normal Distribution of Total Mass

DOI: 10.13009/EUCASS2025-185

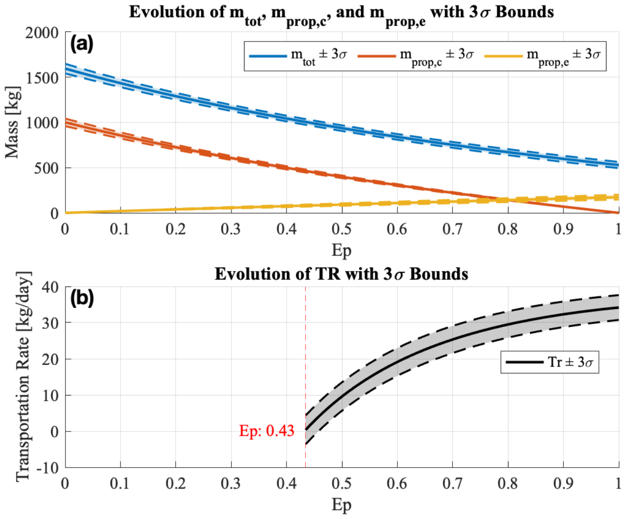

Figure 15: 3-Sigma Analysis

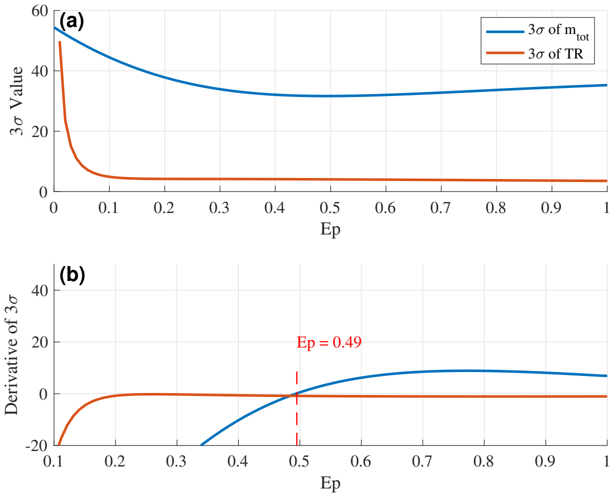

Figure 16: 3σ distribution for different EP fractions.

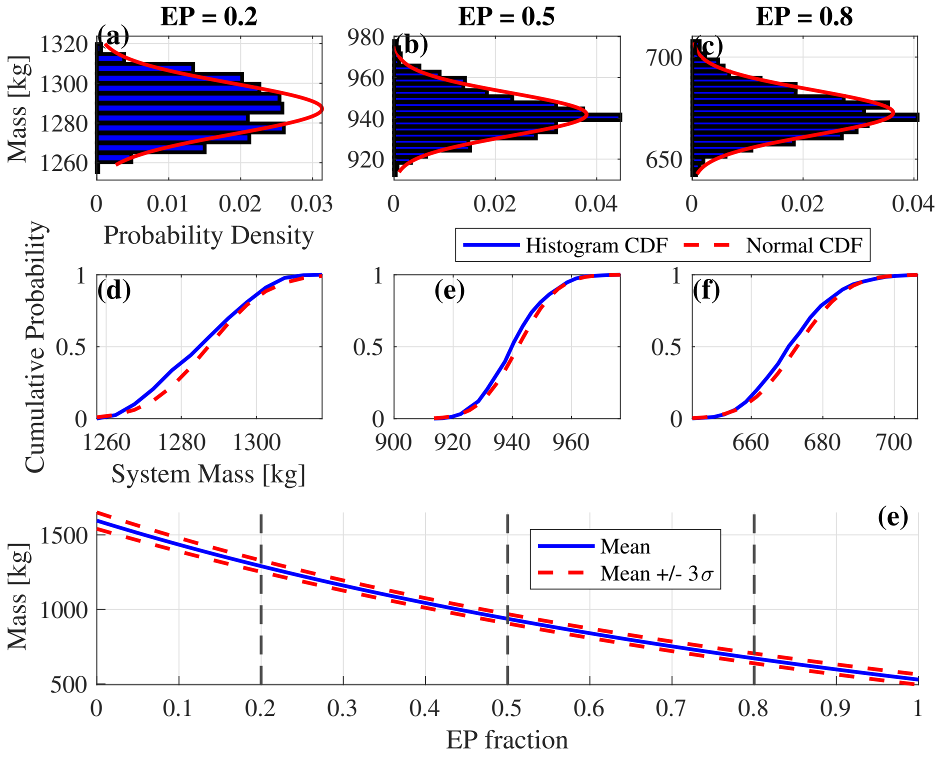

Figure 17: Probability Distribution of Total Propulsion System Mass

5. Conclusions

The main aim of this research was to provide a flexible design analysis framework for evaluating multimode thrusters. The work is structured to provide a discussion with existing literature by presenting results relative to a benchmark mission.[10] Additionally, the analysis focuses on technologies with the potential for near-term mission implementation — specifically, electrothermal arcjet–monopropellant combinations.

The study reveals that the total system mass across different electric propulsion fractions may have been previously underestimated, due to the contribution of power generation systems (e.g., solar panels). The results indicate that the total propulsion system mass can reach approximately 1500 kg for an EP fraction of 0, and 500 kg for an EP fraction

DOI: 10.13009/EUCASS2025-185

of 1 (assuming a 500 kg payload for LEO–GEO transfer). Similarly, the transportation rate was estimated as 36 kg/day for systems operating in fully electric mode. While only at EP fraction of 0.39 transportation rate becomes positive.
The analysis was further extended to examine the impact of input parameter uncertainties on system-level outputs. This includes a technical implementation of Monte Carlo simulations, convergence studies, and an assessment of how key parameter variability affects overall system performance. Results show a strong correlation between variability in the specific impulse of electric propulsion and both total system mass and transportation rate. The onset of high correlation occurs at an EP fraction of approximately 0.38 for total mass and 0.2 for transportation rate. Uncertainty in total system mass reaches a minimum near an EP fraction of 0.49, suggesting an optimal trade-off between performance and robustness. This insight may serve as a valuable guideline for designers seeking to minimize risk while maximizing efficiency in multimodal mission architectures. Additionally, if the uncertainties are included in the analysis, the transportation rate takes a positive value only at 0.43.
Overall, this research contributes to the ongoing discussion on the role of multimode thrusters in in-space propulsion. It provides a deeper understanding of how design decisions, subsystem modeling choices, and parameter uncertainty interact in the context of multimode propulsion systems. The insights gained here not only improve existing methodologies but also pave the way for more informed and resilient mission design practices in future spacecraft development.

Acknowledgments

The authors would like to thank David Samolkin for valuable discussions throughout the development of this work, and Avinash Rao for helpful comments that improved the quality of the paper.

References

[1] Joshua L. Rovey, Christopher T. Lyne, Alex J. Mundahl, Nicolas Rasmont, Matthew S. Glascock, Mitchell J. Wainwright, and Steven P. Berg. Review of Multimode Space Propulsion. *Progress in Aerospace Sciences*, 118:100627, 2020.

[2] Steven Berg and Joshua Rovey. Assessment of Multi-Mode Spacecraft Micropropulsion Systems. In *50th AIAA/ASME/SAE/ASEE Joint Propulsion Conference*, 07 2014.

[3] Bryan Cline, Steven Berg, and Joshua Rovey. Preliminary Screening of Multimode Spacecraft Propulsion Systems for Interplanetary Missions. In *AIAA SCITECH 2022 Forum*, 01 2022.

[4] Giusy Falcone, Daniel L. Engel, Marta Cortinovis, Charles N. Ryan, Joshua Lucas Rovey, Zachary R. Putnam, Steven P. Berg, and Michael F. Lembeck. Mission Performance Assessment of Multimode Propulsion for Satellite Servicing Applications. *2022 IEEE Aerospace Conference (AERO)*, pages 1–19, 2022.

[5] Bryan C. Cline, Alex Pascarella, Robyn M. Woollands, and Joshua L. Rovey. Indirect optimal control techniques for multimode propulsion mission design. *Acta Astronautica*, 223:759–776, 2024.

[6] Animesh Sharma, Anthony C. Adducci, Joshua Rovey, Chengyu Ma, Charles N. Ryan, Steven Berg, Michael Lembeck, and Zachary R. Putnam. *Green Ionic Liquid Multimode Monopropellant Based Chemical Microthruster*.

[7] P. Mallalieu and M. Jugroot. Multimodal electrospray thruster for small spacecraft: design and experimental characterization. *Journal of Electric Propulsion*, 3:12, 2024.

[8] Ewan Fonda-Marsland and Charlie Ryan. Preliminary Ionic Liquid Propellant Selection for Dual-Mode Micro-Propulsion Systems. 07 2017.

[9] David Samolkin and Steven Berg. Performance Estimations of Multi-Mode Spacecraft Propulsion Utilizing Decomposed Monopropellants. In *AIAA SCITECH 2025 Forum*, 2025.

[10] Steven P. Berg and Joshua Lucas Rovey. Assessment of High-Power Electric Multi-Mode Spacecraft Propulsion Concepts. In *33rd International Electric Propulsion Conference in Washington D.C, USA*, 2013.

[11] B. Wollenhaupt, Q. H. Le, and G. Herdrich. Overview of thermal arcjet thruster development. *Aircraft Engineering and Aerospace Technology*, 90(2):280–301, 2018.

[12] Steven P. Berg. *Development of ionic liquid multi-mode spacecraft micropropulsion systems*. PhD thesis, Missouri University of Science and Technology, 2015.

DOI: 10.13009/EUCASS2025-185

[13] Davide Vetralla. Design Analysis of Multimode Propulsion Systems Utilizing Green Monopropellants. Master's thesis, Politecnico di Milano, 2025.

[14] R. W. Humble, G. N. Henry, and W. J. Larson. *Space Propulsion Analysis and Design*. McGraw-Hill, 1995.

[15] B. Melloe, C. Smith, K. Carr, and R. Bellis. Hydrazine storage in critical applications - a 10-year milestone. In *29th Joint Propulsion Conference and Exhibit*, 1993.

[16] S. Godron and B. J. McBride. Computer Program for Calculation of Complex Chemical Equilibrium Compositions and Applications, 1996. NASA Reference Publication 1311.

[17] George P. Sutton and Oscar Biblarz. *Rocket Propulsion Elements*. Wiley, 9th edition, 2016.

[18] Angelo Cervone, Lucio Torre, Luca d'Agostino, Antony J. Musker, Graham T. Roberts, Cristina Bramanti, and Giorgio Saccoccia. Development of Hydrogen Peroxide Monopropellant Rockets. In *42nd AIAA/ASME/SAE/ASEE Joint Propulsion Conference & Exhibit*. American Institute of Aeronautics and Astronautics, 2006. AIAA 2006-5239.

[19] Redha Amri, D. Gibbon, and T. Rezoug. The design, development and test of one newton hydrogen peroxide monopropellant thruster. *Aerospace Science and Technology*, 25:266–272, 2013.

[20] Moog Inc. Monopropellant Thrusters – Product Overview. `https://www.moog.com/space`, 2024. Product brochure, Form 500-934 0424.

[21] Filippo Maggi. Lecture Slides for Space Propulsion. Lecture slides, 2022. Course taught at Politecnico di Milano, Academic Year 2022–2023.

[22] NASA Small Spacecraft Systems Virtual Institute. State-of-the-Art Small Spacecraft Technology: Power Subsystems, 2024. Accessed: 2025-05-01.

[23] Aerojet Rocketdyne. MR-510 Arcjet Thruster, 2025. Accessed: 2025-05-01.

[24] ExoTerra Corporation. Fold-Out Solar Arrays - Product Overview, 2023. Accessed 2025-05-02.

[25] Preyansh Malaviya, Vishwadeep Sarvaiya, Abhishek Shah, Drupad Thakkar, and Manan Shah. A comprehensive review on space solar power satellite: an idiosyncratic approach. *Springer-Verlag GmbH Germany, part of Springer Nature*, 2022.

[26] Redwire Corporation. Solar arrays – roll out solar array (rosa). Redwire Corporation, Product Brochure, 2021. Accessed: 2025-05-01, URL: `https://www.redwirespace.com`.

[27] Rao Surampudi, Tom Hamilton, Donald Rapp, Paul Stella, Nick Mardesich, Jack Mondt, Bill Nesmith, Robert L. Bunker, James Cutts, Sheila G. Bailey, Henry B. Curtis, Mike Piszczor, Ed Gaddy, Dean Marvin, and Larry Kazmerzki. Solar Cell and Array Technology for Future Space Science Missions. NASA-JPL, NASA-GRC, NASA-GSFC, DOE-NREL, Aerospace Corp., 2002. Written by Team Members, June 2002.

[28] Todd Bayer, Molly Bittner, Brent Buffington, Gregory Dubos, Eric Ferguson, et al. Europa clipper mission: Preliminary design report. In *2019 IEEE Aerospace Conference*, pages 1–24, 2019.

[29] Thomas W. Haag and Francis M. Curran. High-Power Hydrogen Arcjet Performance. Technical Report NASA TM-105143, AIAA-91-2226, NASA Lewis Research Center, 1991. Prepared for the 27th Joint Propulsion Conference, Sacramento, CA, June 24–27, 1991.

[30] Kento Shirasu, Hiroki Kuwabara, Masayuki Matsuura, Hiroyuki Koizumi, Yuichi Nakagawa, Hiroki Watanabe, and Hokuto Sekine. Demonstration and experimental characteristics of a water-vapor Hall thruster. *Journal of Electric Propulsion*, 2, 03 2023.

[31] Ronald W. Shonkwiler and Franklin Mendivil. *Explorations in Monte Carlo Methods*. Undergraduate Texts in Mathematics. Springer Nature Switzerland AG, Cham, Switzerland, 2 edition, 2024. 2nd edition. Mathematics Subject Classification: 65C05, 68T05, 60J20, 60G40.

[32] K. J. Davidian, R. H. Dieck, and I. Chuang. A Detailed Description of the Uncertainty Analysis for High Area Ratio Rocket Nozzle Tests at the NASA Lewis Research Center. NASA Technical Memorandum NASA-TM-100203, NASA Lewis Research Center, 1987.

DOI: 10.13009/EUCASS2025-185

[33] Davide Viganò, Adriano Annovazzi, and Filippo Maggi. Monte Carlo Uncertainty Quantification Using Quasi-1D SRM Ballistic Model. *International Journal of Aerospace Engineering*, 2016:8, 2016.

[34] Davide Viganò. Monte Carlo Method for Uncertainty Quantification of SRM Internal Ballistic Model. Laurea specialistica thesis, Politecnico di Milano, Scuola di Ingegneria Industriale, Dipartimento di Scienze e Tecnologie Aerospaziali, Milan, Italy, 2014. Relatore: Prof. F. Maggi. Anno Accademico 2013–2014. Matricola 787058.